

# Stabilization of colloidal Ti, Zr, and Hf oxide nanocrystals by protonated tri-*n*-octylphosphine oxide (TOPO) and its decomposition products.

Katrien De Keukeleere,<sup>1</sup> Sofie Coucke,<sup>1</sup> Els De Canck,<sup>1</sup> Pascal Van Der Voort,<sup>1</sup> Fabien Delpéch,<sup>2</sup> Yannick Coppel,<sup>3</sup> Zeger Hens,<sup>1</sup> Isabel Van Driessche,<sup>1</sup> Jonathan S. Owen,<sup>4</sup> Jonathan De Roo<sup>1,4\*</sup>

<sup>1</sup> Department of Inorganic and Physical Chemistry, Ghent University, Gent, Belgium.

<sup>2</sup> INSA, UPS, CNRS, Laboratoire de Physique et Chimie des Nano-Objets (LPCNO), Université de Toulouse, Toulouse, France.

<sup>3</sup> Laboratoire de Chimie de Coordination, CNRS, UPR 8241, Université de Toulouse, Toulouse, France.

<sup>4</sup> Department of Chemistry, Columbia University, New York, USA

Corresponding author: Jonathan De Roo – [jd3355@columbia.edu](mailto:jd3355@columbia.edu)

## ***Abstract***

Although TiO<sub>2</sub>, ZrO<sub>2</sub> and HfO<sub>2</sub> nanocrystals are often synthesized in tri-*n*-octylphosphine oxide (TOPO), it is unclear whether TOPO also serves as ligand. Using liquid and solid state <sup>1</sup>H and <sup>31</sup>P nuclear magnetic resonance spectroscopy and X-ray fluorescence spectroscopy, we show that the nanocrystal surface is capped by several derivatives of TOPO. In the <sup>31</sup>P NMR spectrum, di-*n*-octylphosphinate ( $\delta = 57$  ppm) and P,P'-(di-*n*-octyl) pyrophosphonate ( $\delta = 20$  ppm) are found coordinated to the nanocrystal. In addition, hydrogen chloride associates with the metal oxide nanocrystal surface and protonates TOPO. The resulting hydroxyl-tri-*n*-octylphosphonium, [HO-PR<sub>3</sub>]<sup>+</sup>, is tightly associated with the nanocrystal surface ( $\delta(^{31}\text{P}) = 73$  ppm) due to electrostatic interactions and hydrogen bonding. To simplify the complex surface composition, we exchange the original surface species for carboxylate or phosphonate ligands. The protonation of TOPO is an unexpected example of lyophilic ion pairing between an acidic metal oxide nanocrystal and a weakly basic ligand molecule that is formed in nonpolar solution. Our results contrast with the classically envisaged L-type binding motif of TOPO to surface metal ions. The generality of this stabilization mode and its relevance to catalysis is discussed.

# 1. Introduction

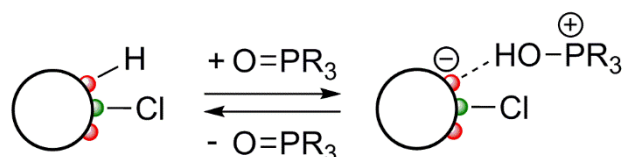
The metal oxides of group 4 ( $\text{TiO}_2$ ,  $\text{ZrO}_2$  and  $\text{HfO}_2$ ) constitute a widely-used class of materials, characterized by a wide band gap, a high melting point, high dielectric constant and excellent chemical and thermal stability.  $\text{TiO}_2$  is used as an electron transporting layer in solar cells<sup>1-4</sup> and LEDs<sup>4</sup> due its low work function and intrinsic *n*-type doping. In addition,  $\text{TiO}_2$ ,<sup>5-10</sup>  $\text{ZrO}_2$ <sup>11-12</sup> and  $\text{HfO}_2$ <sup>13</sup> nanostructures are involved in (photo)catalytic processes and display photoluminescence associated with either defects or dopants.<sup>14-17</sup> Due to their high thermal and chemical stability,  $\text{ZrO}_2$  and  $\text{HfO}_2$  nanocrystals (NCs) are used in superconducting nanocomposites<sup>18-19</sup> and oncology.<sup>20</sup>  $\text{HfO}_2$  is employed in  $\gamma$ -ray scintillators for its high absorption cross section.<sup>21</sup> Because of their high refractive index, all group IVB metal oxides find applications in optical nanocomposites.<sup>22-27</sup> In these examples and others,<sup>28</sup> the surface chemistry, *i.e.*, the coordination of organic ligands to nanocrystal surfaces,<sup>29</sup> is key to their function and is often determined by the synthesis route.

Many syntheses of group 4 metal oxide NCs have been developed, yielding materials of varying quality. Aqueous syntheses occur quickly and typically give NCs with poor particle size distributions and low crystallinity.<sup>10, 30</sup> Syntheses in benzyl alcohol solution produce highly crystalline but aggregated NCs<sup>14, 25, 31-35</sup> that can be dispersed with surfactants.<sup>36-38</sup> Both the NC size<sup>14, 31, 33</sup> and crystal structure<sup>39</sup> can be tuned by varying the metal precursor. A variety of group 4 metal oxide NCs can also be synthesized in organic surfactants, including oleylamine<sup>21, 23</sup> or tri-*n*-octylphosphine oxide (TOPO). For example,  $\text{TiO}_2$  and  $\text{ZrO}_2$  NCs were recently synthesized from a mixture of the corresponding metal halide and metal alkoxide in TOPO and heptadecane.<sup>40,16</sup>  $\text{HfO}_2$  nanorods<sup>41-43</sup> and solid solutions<sup>42, 44</sup> of  $\text{Hf}_x\text{Zr}_{1-x}\text{O}_2$  can also be synthesized in TOPO. NCs synthesized in TOPO stand out in terms of monodispersity, crystallinity, scalability, and colloidal stability, which is perhaps surprising given the weak Lewis basicity of this solvent.

The surface chemistry of group IVB metal oxide NCs has proven essential to nanocrystal assembly,<sup>45</sup> charge transport in nanocrystalline solar cells,<sup>1</sup> and their activity as photocatalysts.<sup>46</sup> For these reasons, the surface chemistry of  $\text{ZrO}_2$  and  $\text{HfO}_2$  NCs, particularly with carboxylic acid ligands, has been carefully studied.<sup>38, 47-48</sup> On the other hand, the surface chemistry of metal oxide NCs synthesized in TOPO, is less well understood.<sup>1, 6-8, 45-46, 49-50</sup> It is unclear whether TOPO is the surface ligand, particularly given a recent study showing that stoichiometric CdSe NCs are unstable to aggregation in neat TOPO.<sup>51</sup> Furthermore, it was

reported that wurtzite CdSe NCs, synthesized in TOPO, are bound by phosphinic and phosphonic acid impurities in the TOPO surfactant.<sup>52-55</sup> Therefore, we sought to understand whether TOPO acts as the stabilizing ligand for metal oxide NCs synthesized in TOPO.

Our studies show that the highly acidic conditions produced by the  $MCl_4$  precursor ( $M = Ti, Zr$  or  $Hf$ ) can convert pure TOPO to octylphosphinic acid and pyrophosphonate, which both bind strongly to the nanocrystal surface. Moreover, hydrogen chloride produced by the precursor conversion associates with the product nanocrystal and protonates TOPO. The latter remains bound to the nanocrystal by hydrogen bonding and electrostatic interactions (Scheme 1). By means of ligand exchange with phosphonic and carboxylic acids, the complex surface composition is simplified and chloride is removed from the dispersion. We thus obtain nanocrystals with well-defined phosphonate ligand shells. This study underscores the importance of lyophilic electrostatic stabilization<sup>51</sup> as a binding motif and suggests protonated TOPO as a potentially interesting ligand for applications in acid catalyzed processes.



**Scheme 1.** Reversible protonation of TOPO by the hydrogen chloride adduct of  $MO_2$  ( $M = Ti, Zr$  or  $Hf$ ).

## 2. Results

Quasi-spherical  $ZrO_2$  NCs, with a tetragonal crystal structure (average diameter = 3.5 nm,  $\sigma = 11\%$ ) are synthesized from  $ZrCl_4$  and  $Zr(OiPr)_4 \cdot iPrOH$  in TOPO according to a published procedure (Figures 1 and S1).<sup>16</sup> Alternatively, to avoid impurities in TOPO and to tackle reproducibility problems associated with the dissolution of  $ZrCl_4$ , we used recrystallized TOPO and the well-defined *bis*-tetrahydrofuran complex,  $ZrCl_4(THF)_2$ . The latter is a white crystalline powder that readily dissolves in TOPO at 80 °C. Following purification, the  $^1H$  nuclear magnetic resonance (NMR) spectrum of a  $ZrO_2$  NC dispersion shows only broadened resonances from surface bound ligands (Figure 1C). These molecules are tightly bound to the NC surface since they are retained in a diffusion filtered spectrum (Figure 1C). A diffusion coefficient of 117  $\mu m^2/s$  was estimated from the mono-exponential decay of the NMR intensity in a diffusion ordered spectroscopy (DOSY) measurement (Figure S2). According to the Stokes-Einstein relation, this diffusion coefficient corresponds to a solvodynamic diameter of

6.3 nm, which agrees with a NC core diameter of 3.5 nm and a ligand shell thickness of 1.4 nm. Dynamic light scattering measurements support a similar solvodynamic diameter (Figure 1D). The organic ligand content in a typical purified sample is  $19 \pm 1$  mass %, which could be measured using thermogravimetric analysis (TGA). From the TGA analysis, the NC diameter, and the concentration of  $\text{CH}_3$  units (30.6 mmol/L) we calculate a NC concentration (280  $\mu\text{mol/L}$ ) and surface ligand density of  $3 \pm 0.5$  alkyl chains  $\text{nm}^{-2}$  (see Supporting Information). Similar coverages have been reported on  $\text{HfO}_2$  and  $\text{CdSe}$  NCs.<sup>38, 56</sup>

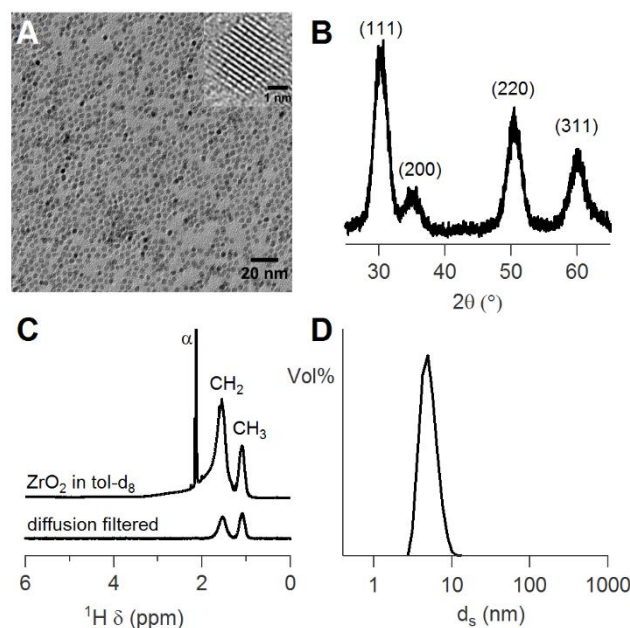


**Figure 1.** (A) TEM, (B) XRD, (C) solution  $^1\text{H}$  NMR spectrum ( $\alpha$  denotes the  $\text{CH}_3$  resonance of toluene) and (D) DLS size distributions of  $\text{ZrO}_2$  NCs, synthesized in TOPO, purified three times and dispersed in toluene.

**Elucidation of the surface chemistry.**  $^{31}\text{P}$  NMR spectroscopy is a powerful method with which to assign the types of surface ligands.<sup>52-53, 57-58</sup> The  $^{31}\text{P}$  NMR spectrum of a  $\text{ZrO}_2$  NC dispersion in toluene- $d_8$ , features three broad peaks centered at 73, 57 and 20 ppm (Figure 2A). This suggests that multiple phosphorus-containing species are bound to the nanocrystals, in contrast to the general assumption of a uniform TOPO capping.<sup>16, 45, 49-50, 59</sup> A variety of chemical tests described below allowed us to assign the resonance at 73 ppm to hydroxyl-tri-*n*-octylphosphonium ( $[\text{HO-PR}_3]^+$ ,  $\text{R} = n\text{-octyl}$ ) cations that are associated with the nanocrystal surface. The other two resonances are assigned to di-*n*-octylphosphinic acid (DOPA,  $\delta = 57$  ppm) and P,P'-(di-*n*-octyl) pyrophosphonate (PPA,  $\delta = 20$  ppm). The relative abundance of the phosphorus species is affected by the relative ratio of  $\text{ZrCl}_4$  and  $\text{Zr}(\text{OiPr})_4 \cdot i\text{PrOH}$  precursors where a ratio of 1.25:1 leads to a maximal content of  $[\text{HO-PR}_3]^+$  (Figure S3).

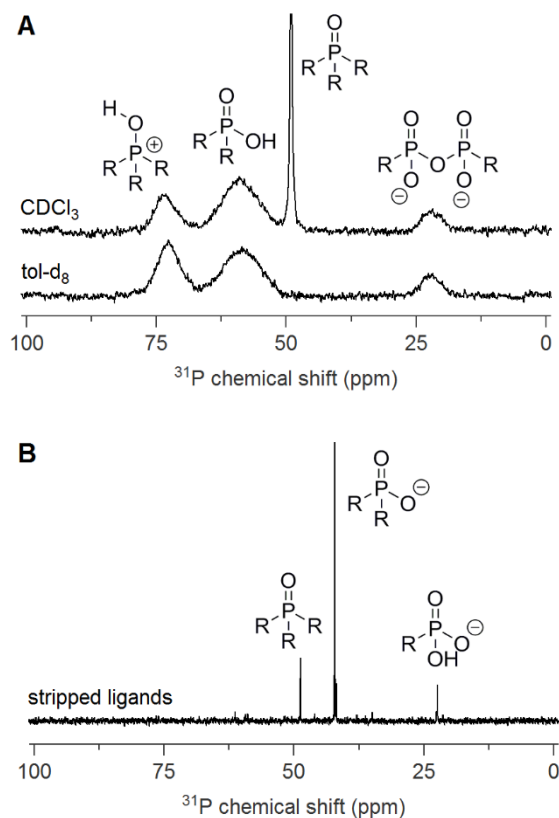
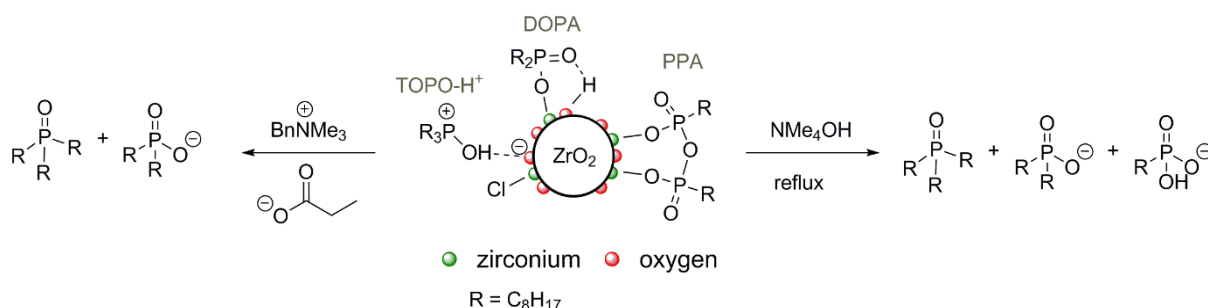


**Figure 2.** (A) Solution  $^{31}\text{P}$  NMR spectra of  $\text{ZrO}_2$  NCs in toluene- $d_8$  and  $\text{CDCl}_3$ . The NCs are synthesized with a 1:1 mixture of  $\text{ZrCl}_4$  and  $\text{Zr}(\text{iPrO})_4 \cdot \text{iPrOH}$ . (B) Ligands stripped from  $\text{ZrO}_2$  NCs by refluxing in methanol/water with tetramethylammonium hydroxide, dissolved in  $\text{CDCl}_3$ .

Several observations support the assignment of surface associated  $[\text{HO-PR}_3]^+$  to the resonance at  $\delta = 73$  ppm. First, a similar chemical shift is observed in  $\text{CDCl}_3$  solutions of TOPO and trifluoroacetic acid. Second, when the  $\text{ZrO}_2$  NCs are transferred from toluene- $d_8$  to  $\text{CDCl}_3$ , sharp  $^1\text{H}$  and  $^{31}\text{P}$  resonances appear ( $\delta = 48$  ppm) that correspond to freely diffusing, neutral TOPO (Figure 2A, S4 and S5).<sup>52, 55</sup> Concomitantly, the resonance at  $\delta = 73$  ppm decreases in intensity, thus proving that it is derived from (protonated) TOPO. Similarly, TOPO desorbs upon heating NCs in dichlorobenzene- $d_4$  to 130 °C and reverts to the protonated state at lower temperatures. This behavior in chloroform or at elevated temperatures is consistent with the equilibrium shown in Scheme 1. Furthermore, using X-ray fluorescence measurements, chloride can be observed in the purified nanocrystals (Figure S6). These anions help provide charge balance for the associated  $[\text{HO-PR}_3]^+$  and suggest that it is electrostatically associated with a negatively charged NC (Scheme 1).

To assign the other  $^{31}\text{P}$  NMR signals, benzyltrimethylammonium propionate<sup>52</sup> and tetramethyl ammonium hydroxide were used to displace the ligands (Scheme 2). For example, benzyltrimethylammonium propionate releases TOPO and di-*n*-octylphosphinate ( $\delta = 40$  ppm),

causing a decrease in the broad resonances at 73 and 57 ppm (Figure S7). Refluxing the ZrO<sub>2</sub> NCs in a solution of methanol/water and tetramethylammonium hydroxide (see Scheme 2 and experimental section) removes all the phosphorus containing ligands. In addition to TOPO and di-*n*-octylphosphinate, the <sup>31</sup>P NMR spectrum now features a resonance from *n*-octylphosphonate ( $\delta = 22$  ppm) (Figure 2B). Alternatively, hydrolysis of P,P'-(di-*n*-octyl)pyrophosphonic acid (an anhydride of *n*-octylphosphonic acid) can explain the result. Given the strong binding affinity and reported chemical shift of alkylphosphonates bound to zirconia (25 ppm),<sup>60-61</sup> we attribute the 20 ppm resonance to P,P'-(di-*n*-octyl)pyrophosphonate. Our assignment is confirmed by the appearance of pyrophosphonate upon exchange with phosphonic acids (*vide infra*) and by the increase of the 20 ppm resonance upon addition of separately synthesized P,P'-(di-*n*-dodecyl)pyrophosphonate (Figure S8). However, we cannot fully exclude traces of *n*-octylphosphonate. It is important to note that while phosphinic and phosphonic acids are often found as impurities in TOPO,<sup>54-55</sup> the above ligands do not originate from the used TOPO since the TOPO solvent has been recrystallized and the impurities removed (see experimental section).<sup>53</sup> However, we still retrieve phosphinic and phosphonic acids on the nanocrystal surface, and therefore, we infer that these ligands arise from the decomposition of TOPO under the highly Lewis and Brønsted acidic conditions.



**Scheme 2.** The binding of TOPO, DOPA and PPA to ZrO<sub>2</sub> NCs. Note the stoichiometry of the surface; stoichiometric for TOPO and DOPA binding sites and cation rich for PPA binding sites. Also, the stripped ligands are displayed upon addition of benzyltrimethylammonium propionate or after reflux in water/methanol solution of tetramethylammonium hydroxide.

Having identified three phosphorus containing surface ligands, we set out to identify the extent to which these ligands are protonated. The solid state cross polarization magic angle spinning (CP-MAS) <sup>31</sup>P NMR spectrum and a solid state <sup>1</sup>H-<sup>31</sup>P heteronuclear correlation spectrum of dried ZrO<sub>2</sub> nanocrystals are shown in Figure 3. The line shape resembles the solution state spectrum in toluene-*d*<sub>8</sub>. Cross peaks can be observed between the phosphorus resonances of [HO-PR<sub>3</sub>]<sup>+</sup>, di-*n*-octylphosphinate, and a broad <sup>1</sup>H signal centered near 6 ppm. This signal is presumably a convolution of multiple acidic hydrogens in the sample. A resonance at a similar

chemical shift was previously assigned to a hydroxyl group on the surface of  $ZrO_2$ .<sup>60, 62</sup> In contrast, the pyrophosphonate signal has little cross correlation with the  $^1H$  NMR spectrum. Based on these cross correlations we tentatively conclude that di-*n*-octylphosphinate adsorbs on the oxide surface and forms a hydrogen bond to surface hydroxyls, while the pyrophosphonate ligands do not participate in hydrogen bonding (Scheme 2). Our assignment of the deprotonated anionic ligand form is consistent with the following arguments: (1) the ligands are not removed by the purification process, suggesting they are not simply datively bound phosphinic or phosphonic acids, and (2) coordination to Lewis acidic zirconium centers will stabilize the phosphinate and phosphonate anions over their protonated phosphinic and phosphonic acid forms. This assignment is analogous to the dissociation of carboxylic acids on  $ZrO_2$  and  $HfO_2$  NC surfaces reported previously.<sup>29, 38, 62</sup>

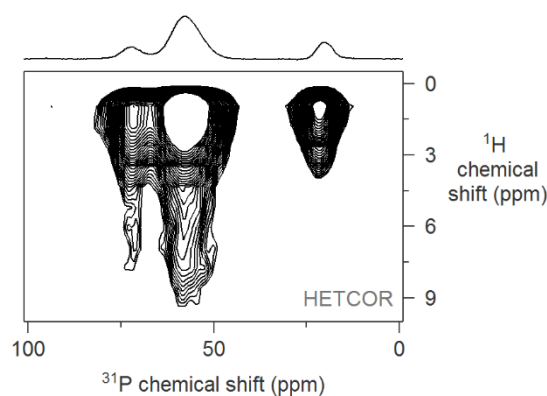


**Figure 3.**  $^{31}P$  CP MAS solid state NMR spectrum of the  $ZrO_2$  NC powder. 18 kHz spinning rate, 1 ms contact time and the HETCOR spectrum, 1 ms contact time

**Generality of surface chemistry model.** To investigate the generality of our conclusions,  $TiO_2$  and  $HfO_2$  nanocrystals were synthesized according to the same strategy. Both types of NCs are slightly elongated and the final size is about  $9.1 \pm 2.3$  nm for  $TiO_2$  and  $8 \text{ nm} \pm 2.4$  nm for  $HfO_2$ , both larger than the  $ZrO_2$  NCs (Figure 4). The larger size and the irregular surface causes even broader NMR signals, so highly concentrated samples were required to obtain  $^{31}P$  NMR spectra with sufficient signal to noise. A similar distribution of ligands is found, including  $[HO-PR_3]^+$  ( $\delta = 73$  ppm) and di-*n*-octylphosphinate ( $\delta = 57$  ppm). To unambiguously demonstrate their identity, the ligands were displaced by ammonium carboxylate (Figure S9). Pyrophosphonate ligands were not detected in the  $TiO_2$  sample, while a measurable amount is found in the  $HfO_2$  sample. The difference may reflect the greater acidity of the transition metal halide complexes and their ability to activate TOPO toward decomposition.

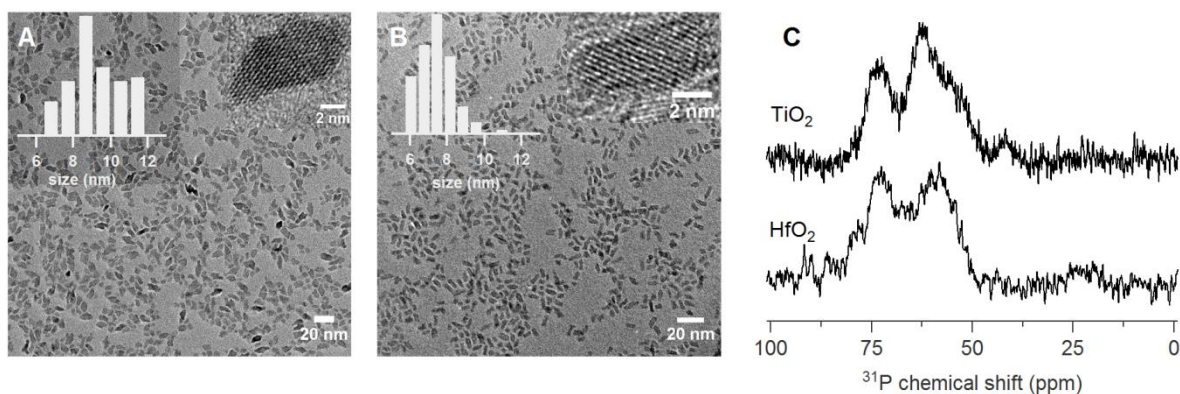


**Figure 4.** (A) TiO<sub>2</sub> NCs (B) HfO<sub>2</sub> NCs and (C) The <sup>31</sup>P spectrum of TiO<sub>2</sub> (with [HO-PR<sub>3</sub>]<sup>+</sup> and di-*n*-octylphosphinic acid). The small peak at 45 ppm is most likely TOPO that is not tightly bound but in dynamic exchange. The <sup>31</sup>P spectrum of HfO<sub>2</sub> NCs (with [HO-PR<sub>3</sub>]<sup>+</sup>, di-*n*-octylphosphinic acid and pyrophosphonate).

**Ligand exchange for carboxylic acids.** On the basis of these assignments, we sought to perform a ligand exchange to simplify the ligand shell of the ZrO<sub>2</sub> NCs, since its complexity can obscure structure-function relationships.<sup>46</sup> In addition, we sought methods that remove hydrogen chloride, which is not easily removed from nanocrystalline thin films using O<sub>2</sub>/plasma treatments.<sup>45, 49</sup> For these reasons we explored the exchange of surface ligands under basic conditions (Figure 5). Adding *n*-octylamine to a ZrO<sub>2</sub> NC dispersion in chloroform liberates neutral TOPO molecules from the surface and di-*n*-octylphosphinate partially desorbs (Figure 5B), most likely as an *n*-octylammonium ion pair.<sup>48, 51</sup> Addition of oleic acid with the *n*-octylamine more completely removes the di-*n*-octylphosphinate from the surface along with the TOPO, although the pyrophosphonate ligands remain intact (Figure S10 and S11). Following purification and isolation of the ligand exchange product, the <sup>1</sup>H NMR spectrum of the dispersion carries the finger print of surface bound oleyl chains (Figure 5C), while the XRF spectrum lacks the signals from chloride (Figure S12). We conclude that the amine deprotonates the [HO-PR<sub>3</sub>]<sup>+</sup> ions, liberating TOPO from the nanocrystal, and carboxylate anions displace the di-*n*-octylphosphinate and chloride ligands. Moreover, we conclude that the carboxylate anions do not preferentially displace the pyrophosphonate ligands, suggesting they have especially strong affinity for the ZrO<sub>2</sub> NC surface. However, in the case of TiO<sub>2</sub> NCs, which lack pyrophosphonate ligands (Figure 4), we could prepare a pure carboxylate ligand shell (Figure S13).

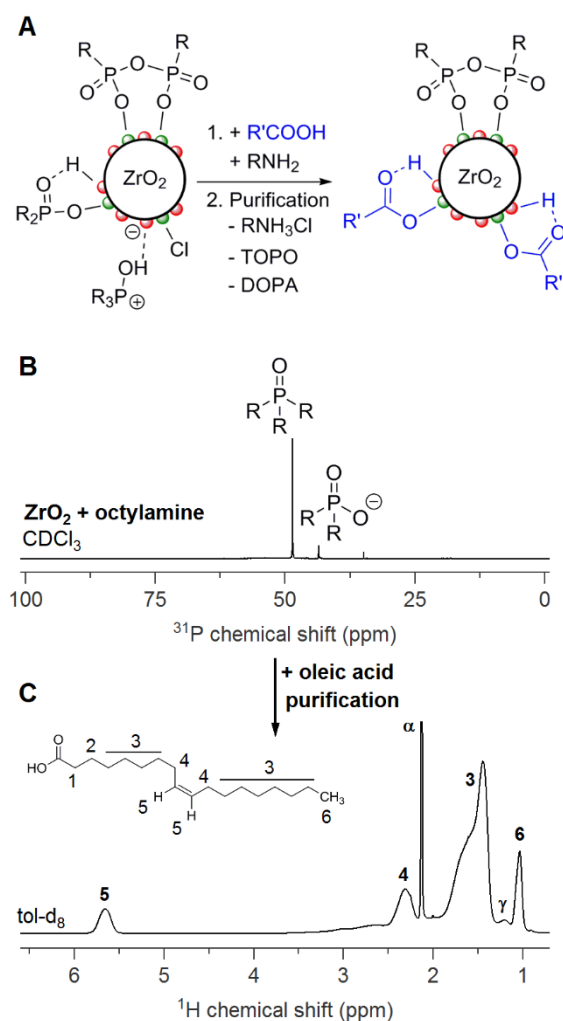


**Figure 5.** (A) Exchange for carboxylic acids under basic conditions. (B) <sup>31</sup>P NMR spectrum of ZrO<sub>2</sub> NCs + octylamine. (C) <sup>1</sup>H NMR spectrum of the purified NCs capped with oleic acid in toluene-*d*<sub>8</sub>. The α resonance is assigned to CH<sub>3</sub> of toluene and the γ resonance is assigned to the octyl chain CH<sub>3</sub>.

The addition of citric acid – without base – stabilizes ZrO<sub>2</sub> NCs in methanol.<sup>19</sup> However, this ligand exchange strategy leads to a complex mixture, because the acidic nanocrystals simultaneously catalyze the esterification of citric acid by methanol. Consequently, the mono-, di- and trimethylated citric acid cause a complex pattern in the <sup>1</sup>H NMR spectrum ( $\delta = 2.5 - 3$  ppm), but are nonetheless separate from the resonances of the native ligands ( $\delta = 0.5 - 2$  ppm) (Figure 6). Interestingly, in the diffusion filtered spectrum, there is a new resonance at 3.6 ppm for the methyl ester (Figure 6). We thus infer that the mono or double ester of citric acid is bound to the surface through the remaining carboxylate functionality. In the <sup>31</sup>P NMR spectrum only one sharp resonance, corresponding to neutral TOPO, is observed (Figure S14). Therefore, we conclude that the phosphonic and phosphonic acids remain tightly bound to the surface and partially esterified citric acid only displaces TOPO.

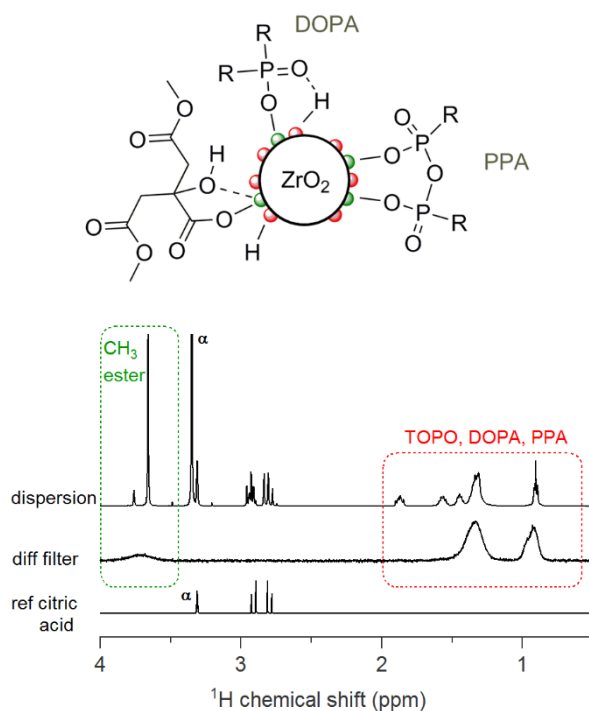


**Figure 6.**  $^1\text{H}$  NMR spectra of a  $\text{ZrO}_2$  NCs dispersion in methanol- $d_4$ , the diffusion filtered spectrum of the dispersion and the reference spectrum of citric acid. The resonance indicated by alpha ( $\alpha$ ) corresponds to the solvent; methanol.

**Ligand exchange for phosphonic acids.** Given the greater affinity of the phosphonic acid ligands for the surface, we studied ligand exchange using *n*-octadecylphosphonic acid (ODPA) (Figure 7). Adding ODPA to  $\text{ZrO}_2$  NCs displaces all the native ligands leaving ODPA capped NCs that could be isolated by precipitation and separated from the TOPO and phosphinate byproducts. This approach produces a signal for a free pyrophosphonate (Figure 7B), consistent with our assignment above, rather than a surface bound *n*-octylphosphonate. The  $^{31}\text{P}$  NMR spectrum of the purified nanocrystal dispersion contains one broad resonance, corresponding to bound ODPA (Figure 7C). XRF measurements demonstrate that the ligand exchange and purification procedure effectively removes remaining chloride ions (Figure S15). In addition, the  $^1\text{H}$  NMR spectrum is free from the sharp signals of freely diffusing ligands, indicating a successful purification (Figure S16). We conclude that the surface ligands are completely converted to tightly bound *n*-octadecylphosphonate ligands, providing a well-defined nanocrystal product.

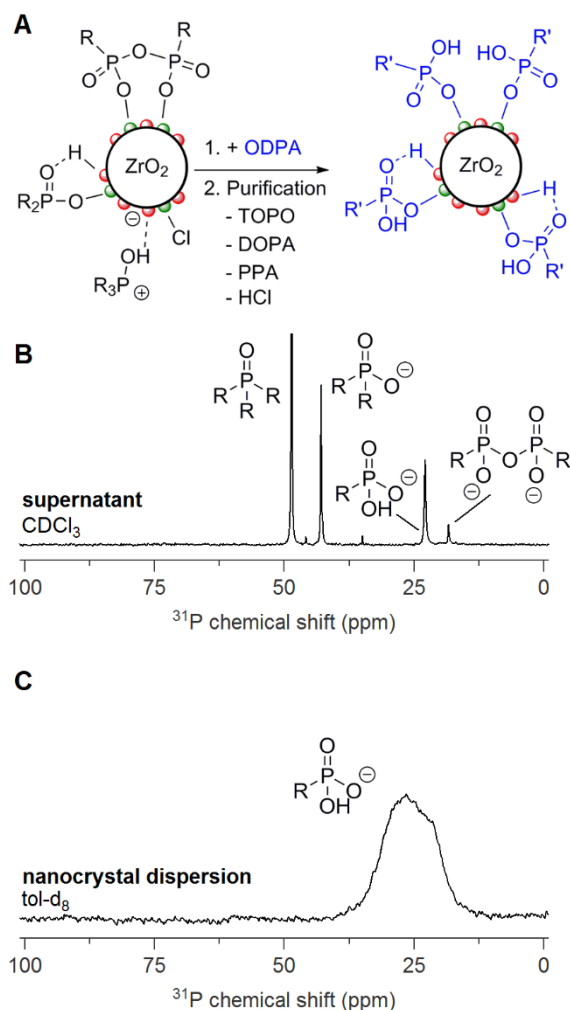


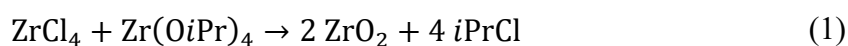
**Figure 7.** (A) Exchange for *n*-octadecyphosphonic acid (ODPA). (B)  $^{31}\text{P}$  NMR spectrum of the supernatant in  $\text{CDCl}_3$  after addition of excess of ODPA to  $\text{ZrO}_2$  NCs and purification. (C)  $^{31}\text{P}$  NMR spectrum of the purified dispersion in toluene- $d_8$ .

### 3. Discussion

Although initially assumed to be bound by L-type TOPO ligands, CdSe nanocrystals turned out to be stabilized by phosphinic and/or phosphonic acid impurities in TOPO.<sup>54-55, 63</sup> Ever since, the status of TOPO as a ligand has been under siege, especially given the recent report that stoichiometric CdSe NCs are unstable in neat molten TOPO.<sup>51</sup> Here, we show that TOPO is not inert nor a simple L-type ligand. Under the acidic conditions used to synthesize  $\text{TiO}_2$ ,  $\text{ZrO}_2$  and  $\text{HfO}_2$ , pure TOPO undergoes decomposition to di-*n*-octylphosphinic acid and P,P'-(di-*n*-octyl) pyrophosphonate that bind the NC surface. Although the precise mechanism is uncertain, it is likely caused by the high Lewis and Brønsted acidity of the reaction mixture. When considering the mass balance of the reaction, the only oxygen source is  $\text{Zr}(\text{O}i\text{Pr})_4 \cdot i\text{PrOH}$  and oxygen is consumed by both metal oxide formation and by conversion of TOPO to phosphinic and

phosphonic acids. Although the formation of byproducts is a characteristic of most chemical reactions, it is especially problematic in nanocrystal syntheses when a byproduct binds to the surface with high affinity, such as in the present case. It is likely that solvent decomposition or surface bound reaction byproducts occur more frequently and this warrants more attention to nanocrystal surface chemistry in synthetic procedures.

The mechanism of non-hydrolytic oxide formation has been investigated in detail<sup>16, 64-65</sup> and the reaction between metal chloride and metal isopropoxide yields isopropyl chloride (Equation 1). Isopropyl chloride can undergo a dehalogenation reaction to form propene<sup>16</sup> (Equation 2) and HCl, hence the source of acidic protons in the reaction mixture.



Hydrogen chloride associates with the nanocrystal and is sufficiently acidic to protonate even weakly basic moieties such as TOPO;  $\text{pK}_a(\text{HO-PR}_3)^+ = -1.5$  (in sulfuric acid).<sup>66</sup> The  $[\text{HO-PR}_3]^+$  is then electrostatically associated with the nanocrystal, creating an unexpected example of lyophilic electrostatic stabilization.<sup>51</sup> Considering the weak basicity of TOPO, it is reasonable to imagine that many metal, semiconductor and metal oxide nanocrystal syntheses,<sup>21, 23, 67-71</sup> performed in even more basic solvents such as oleylamine, may display a similar motif. Here however, the NMR active phosphorus nucleus allowed us to study the fate of the protonated moiety in more detail than could be done for *e.g.*, ammonium compounds. For the same reason, tri-*n*-alkylphosphine oxides have been used as probe molecules to assess the acidity of metal oxides used in heterogeneous acid catalysis.<sup>72-74</sup> Typically, protonated phosphine oxides form a hydrogen bond to the oxide surface,<sup>73</sup> and thus the electron cloud is sensitive to the extent of proton transfer. Consequently, the <sup>31</sup>P chemical shift reflects the acidity of the surface with higher chemical shifts representing more acidic surfaces. The chemical shift observed in our samples of ZrO<sub>2</sub> NCs ( $\delta = 73$  ppm) is indicative of a strongly acidic surface, although not as acidic as sulfonated zirconia ( $\delta = 94$  ppm).<sup>74</sup> The latter is the most powerful solid state acid known and it is particularly active in hydrocarbon isomerization, alkylation and esterification.<sup>75-76</sup> Nevertheless, given the high acidity of the NC surface and their high surface to volume ratio, these NCs might be of interest for acid catalysis. Although in nano-catalysis, ligands – needed for colloidal stability – often block catalytically active surface sites,<sup>77-78</sup> the desorption of TOPO at high temperatures or in more polar solvents is encouraging since this leaves the acidic surface bare for catalytic substrates to bind.

Finally, our attempts to displace the original ligands using carboxylic acids and amines, neutralizes the  $[\text{HO-PR}_3]^+$ , liberates TOPO, and also liberates di-*n*-octylphosphinate and chloride ions. The latter is especially useful since it appeared particularly difficult to remove in earlier reports.<sup>45, 49</sup> Our results are consistent with the previously proposed dissociation of acids on the metal oxide surface, the  $\text{NC}(\text{X})_2$  binding motif.<sup>13, 29, 38</sup> In addition, we found that phosphonates bind better to the surface than carboxylates, which is consistent with the literature on bulk metal oxide surfaces.<sup>60, 79-80</sup> Given the wealth of available phosphonic acids, they seem the most promising candidates to pursue future ligand exchange strategies with.

#### 4. Conclusion

Via a combination of liquid state and solid state NMR, we have demonstrated that group 4 metal oxide nanocrystals synthesized in TOPO contain a variety of ligands including di-*n*-octylphosphinic acid and P,P'-(di-*n*-octyl)pyrophosphonate which form upon decomposition of the TOPO solvent. Moreover, we find that TOPO reacts with Brønsted acid sites on the nanocrystal producing adsorbed  $[\text{HO-PR}_3]^+$  ions that balance charge with the nanocrystal. This motif appears to be a consequence of forming HCl under anhydrous conditions, which adsorbs to the nanocrystal creating a very acidic surface. Basic conditions then neutralize these acids and facilitate desorption of both halide and phosphinate anions and enable partial exchange for oleate ligands. However, the phosphonate ligands are more strongly bound and may only be displaced by other phosphonic acids. This allowed  $\text{ZrO}_2$  nanocrystals to be prepared with a pure *n*-octadecylphosphonic acid ligand shell. These insights fuel the discussion on the status of TOPO as a ligand. In the present case, the very strong acids generated from the group 4 metal halides cause protonation in nonpolar solvent ultimately leading to electrostatically stabilized dispersions, rather than a simple dative ligand binding.

#### 5. Experimental methods

**General considerations.**  $\text{Zr}(\text{O}i\text{Pr})_4 \cdot i\text{PrOH}$  (99.9%),  $\text{ZrCl}_4$  (99.9%),  $\text{Ti}(\text{O}i\text{Pr})_4$  (99.999%),  $\text{TiCl}_4$  ( $\geq 99.0\%$ ),  $\text{Hf}(\text{O}i\text{Pr})_4 \cdot i\text{PrOH}$  (99.9%),  $\text{HfCl}_4$  (99.9%), 25w% solution of  $\text{NMe}_4\text{OH}$  in methanol, oleic acid (technical, 90%), octylamine (99%), toluene (99.5%), acetone (99.8%), methanol (99.8%) were purchased from Sigma Aldrich and used without purification.

Tri-*n*-octylphosphine oxide (99%) was bought from Strem chemicals and recrystallized according to Owen *et al.*<sup>53</sup> The NMR spectra of recrystallized TOPO are shown in Figure S17:  $\{^1\text{H}\}^{31}\text{P}$  NMR (202.5 MHz,  $\text{CDCl}_3$ )  $\delta = 48.5$  ppm.  $\{^1\text{H}\}^{31}\text{P}$  NMR (202.5 MHz, toluene- $d_8$ )  $\delta = 41.5$  ppm.  $\text{ZrCl}_4 \cdot (\text{THF})_2$  was synthesized according to Manzer *et al.*<sup>81</sup> P,P'-(di-*n*-dodecyl)

pyrophosphonic acid was synthesized according to Kopping *et al.*<sup>52</sup> TiO<sub>2</sub> nanocrystals were synthesized according to Trentler *et al.* using 15 g TOPO, 0,6 mL Ti(OiPr)<sub>4</sub> and 0,22 mL TiCl<sub>4</sub> at 300 °C for 10 min.<sup>40</sup> HfO<sub>2</sub> nanocrystals were synthesized according to Tirosh *et al.* using 10 g TOPO, 0.95 g Hf(OiPr)<sub>4</sub>.iPrOH and 0.64 g HfCl<sub>4</sub> at 340 °C for 2 hours.<sup>43</sup> Ligand exchange with citric acid was performed according to Rijckaert *et al.*<sup>19</sup>

For Dynamic Light Scattering (DLS) and zeta potential measurements on suspensions a Malvern Nano ZS was used in backscattering mode (173°). Transmission electron microscopy (TEM) images (of a drop-cast suspension on a grid) were taken on a JEOL JEM-2200FS TEM with Cs corrector. For powder X-ray diffraction (XRD) characterization a Thermo Scientific ARL X'tra X-ray diffractometer was used with the CuK $\alpha$  line as the primary source. XRF measurements were performed on dried suspensions on a Rigaku CG Energy Dispersive X-ray Fluorescence (EDXRF) analyzer.

**Optimized ZrO<sub>2</sub> nanocrystal synthesis, adapted from Joo *et al.*<sup>16</sup>** In a nitrogen filled glovebox, a 50 mL three-neck-flask is loaded with 5 g recrystallized TOPO, Zr(OiPr)<sub>4</sub>.iPrOH (0.775 g, 2 mmol), followed by another 5 g recrystallized TOPO and ZrCl<sub>4</sub>.2THF (0.943 g, 2.5 mmol). A stirring bar is added, and a thermowell, septum and condenser are mounted on the three-neck-flask. The top part of the condenser is sealed with a vacuum adapter for easy connection to the Schlenk line. The setup is taken out of the box and connected to the Schlenk line and the flask is filled with Argon. The temperature is first set to 60 °C to allow the TOPO to melt and all the precursors dissolve easily. The temperature is then raised slowly to 340 °C and held there for 2 hours. After the reaction has completed, the transparent reaction mixture is cooled to 80 °C and toluene (3 mL) is injected. The nanocrystals are purified by the addition of acetone (1: 2 in volume) to the reaction mixture, yielding a white precipitate after centrifugation (3500 rpm – 3 min). The precipitate is suspended in toluene (10 mL) and precipitated with acetone again and redispersed in toluene. The dispersion is centrifuged and filtered (0.25  $\mu$ m PTFE membrane) to discard any insolubles. The resulting suspension is purified two additional times with acetone, and suspended in 10 mL of toluene (25.5 mg ZrO<sub>2</sub> /mL). Yield: 46 %

**Complete ligand removal by tetramethylammonium hydroxide.** 250  $\mu$ L of ZrO<sub>2</sub> NC dispersion (12.5  $\mu$ mol CH<sub>3</sub> units) is evaporated and 2 mL of methanol is added and stirred resulting in a cloudy suspension. 50  $\mu$ L of a 25w% solution of tetramethylammonium hydroxide solution in methanol (119  $\mu$ mol) is added and the suspension is refluxed for 4 hours. Water (2 mL) is added and the suspension is again refluxed for 24 hours. The solvents are removed under

vacuum and 500  $\mu\text{L}$   $\text{CDCl}_3$ , 150  $\mu\text{L}$  oleic acid and 50  $\mu\text{L}$  octylamine are added. The suspension is centrifuged to remove insolubles and the supernatant is measured in NMR (Figure 2B).

**Ligand exchange to oleic acid.** 2 mL of standard  $\text{ZrO}_2$  NC dispersion is dried and 0.6 mL of  $\text{CDCl}_3$  is added. First 20  $\mu\text{L}$  of octylamine is added (NMR analysis) and then 40  $\mu\text{L}$  of oleic acid (NMR analysis). The NCs are precipitated with acetone and redispersed in 200  $\mu\text{L}$   $\text{CHCl}_3$ . 400  $\mu\text{L}$  oleic acid and 200  $\mu\text{L}$  octylamine are added and the NCs are precipitated with 1 mL of acetone. This treatment is repeated and the NCs are dispersed in 200  $\mu\text{L}$   $\text{CHCl}_3$  and 50  $\mu\text{L}$  oleic acid. The NCs are precipitated twice with acetone and redispersed in chloroform. Finally, the NCs are dried and dispersed in toluene- $d_8$ .

**Ligand exchange to *n*-octadecylphosphonic acid.** 2 mL of optimized  $\text{ZrO}_2$  NC dispersion (85  $\mu\text{mol}$   $\text{CH}_3$  units) is dried and dispersed in 0.6 mL of toluene- $d_8$ . 40 mg of octadecylphosphonic acid (120  $\mu\text{mol}$ ) is added and the suspension is subjected to 30 minutes of ultrasound treatment, followed by heating to the boiling point and followed by 30 additional minutes of ultrasound treatment. The NCs are purified three times by precipitation with methanol and redispersion in toluene. To get a clear supernatant, add 2 mL methanol to a 0.5 mL dispersion of NCs and let the NCs settle before centrifugation. The combined supernatant from all the washes is dried and dissolved in  $\text{CDCl}_3$  with octylamine. The NCs are dried and redispersed in toluene- $d_8$ .

**Solution NMR characterization.**<sup>82</sup> Nuclear Magnetic Resonance (NMR) measurements were recorded on Bruker spectrometers operating at a  $^1\text{H}$  frequency of 500.13 MHz. One dimensional (1D)  $^1\text{H}$  and  $^{31}\text{P}$  spectra were acquired using the Bruker pulse sequences zg and zgif (inverse gated decoupling) respectively. For the quantitative 1D  $^1\text{H}$  measurements, 64k data points were sampled with the spectral width set to 16 ppm and a relaxation delay of 30 sec. Concentrations were obtained using the Digital ERETIC method.<sup>83</sup> Diffusion measurements (2D DOSY) were performed using a double stimulated echo sequence for convection compensation and with monopolar gradient pulses; dstegp2s.<sup>84</sup> Smoothed rectangle gradient pulse shapes were used throughout. The gradient strength was varied linearly from 2-95% of the probe's maximum value (calibrated at 50.2 G/cm) in 64 steps, with the gradient pulse duration and diffusion delay optimized to ensure a final attenuation of the signal in the final increment of less than 10% relative to the first increment. The diffusion coefficients were obtained by fitting the Stejskal-Tanner (ST) equation to the signal intensity decay:

$$I = I_0 e^{-(\gamma \delta g \xi)^2 D (\Delta - 0.6 \delta)} \quad (1)$$

with the gyromagnetic ratio of the observed  $^1\text{H}$  nucleus  $\gamma$ , the gradient pulse length  $\delta$ , the gradient strength  $g$ , the diffusion time  $\Delta$  and the diffusion coefficient  $D$ .

**Solid state NMR characterization.** Solid-state NMR experiments were recorded at the LCC (Toulouse) on a Bruker Avance 400 spectrometer equipped with 3.2 mm probes. Samples were spun at 18 kHz at the magic angle using  $\text{ZrO}_2$  rotors.  $^{31}\text{P}$  MAS experiment was performed with a recycle delay of 60 s.  $^{31}\text{P}$  CP MAS spectra were recorded with a recycle delay of 1.5 s and a contact time of 2 ms.  $^{31}\text{P}$  HETCOR were recorded with a recycle delay of 1.5 s and a contact time of 1 ms. All the  $^{31}\text{P}$  spectra were recorded under high-power proton decoupling conditions.  $^{31}\text{P}$  chemical shifts were referenced to an external 85%  $\text{H}_3\text{PO}_4$  sample.

## 6. Associated Content

Supporting information

DOSY decay fittings, XRF measurements, additional NMR spectra. This information is available free of charge via the internet at <http://pubs.acs.org/>

## 7. Author Information

Corresponding author: Jonathan De Roo, [jd3355@columbia.edu](mailto:jd3355@columbia.edu)

The authors declare no competing financial interest.

## 8. Acknowledgements

The authors thank Prof. Ludovico Cademartiri for an insightful discussion at the E-MRS conference. The authors also thank Prof. Dr. José Martins and Dr. Davy Sinnaeve for interesting scientific discussions. The authors thank Dr. Michael Campos for the synthesis of *n*-octadecylphosphonic acid. The NMR equipment used is part of the NMR Expertise Center at Ghent University and was funded in part by the Hercules foundation (AUGE09/006). The authors acknowledge the Belgian American Education Foundation (B.A.E.F.), Fulbright, Ghent University, University of Toulouse, the Région Midi-Pyrénées, the CNRS and the COMPASS project (H2020-MSCA-RISE-2015-691185) for financial support.

## 9. References

1. Boucle, J.; Chyla, S.; Shaffer, M. S. P.; Durrant, J. R.; Bradley, D. D. C.; Nelson, J., Hybrid solar cells from a blend of poly(3-hexylthiophene) and ligand-capped  $\text{TiO}_2$  nanorods. *Adv. Funct. Mater.* **2008**, *18* (4), 622-633.
2. Oregan, B.; Gratzel, M., A LOW-COST, HIGH-EFFICIENCY SOLAR-CELL BASED ON DYE-SENSITIZED COLLOIDAL  $\text{TiO}_2$  FILMS. *Nature* **1991**, *353* (6346), 737-740.

3. Law, M.; Greene, L. E.; Johnson, J. C.; Saykally, R.; Yang, P. D., Nanowire dye-sensitized solar cells. *Nat. Mater.* **2005**, *4* (6), 455-459.
4. Liang, X.; Bai, S.; Wang, X.; Dai, X.; Gao, F.; Sun, B.; Ning, Z.; Ye, Z.; Jin, Y., Colloidal metal oxide nanocrystals as charge transporting layers for solution-processed light-emitting diodes and solar cells. *Chem Soc Rev* **2017**, *46* (6), 1730-1759.
5. Kaniyankandy, S.; Ghosh, H. N., Efficient luminescence and photocatalytic behaviour in ultrafine TiO<sub>2</sub> particles synthesized by arrested precipitation. *J. Mater. Chem.* **2009**, *19* (21), 3523-3528.
6. Chang, S. M.; Lo, P. H.; Chang, C. T., Photocatalytic behavior of TOPO-capped TiO<sub>2</sub> nanocrystals for degradation of endocrine disrupting chemicals. *Appl. Catal. B-Environ.* **2009**, *91* (3-4), 619-627.
7. Chang, S. M.; Hou, C. Y.; Lo, P. H.; Chang, C. T., Preparation of phosphated Zr-doped TiO<sub>2</sub> exhibiting high photocatalytic activity through calcination of ligand-capped nanocrystals. *Appl. Catal. B-Environ.* **2009**, *90* (1-2), 233-241.
8. Chang, S.-m.; Doong, R.-a., Characterization of Zr-Doped TiO<sub>2</sub> Nanocrystals Prepared by a Nonhydrolytic Sol-Gel Method at High Temperatures. *The Journal of Physical Chemistry B* **2006**, *110* (42), 20808-20814.
9. Maijenburg, A. W.; Veerbeek, J.; de Putter, R.; Veldhuis, S. A.; Zoontjes, M. G. C.; Mul, G.; Montero-Moreno, J. M.; Nielsch, K.; Schäfer, H.; Steinhart, M.; ten Elshof, J. E., Electrochemical synthesis of coaxial TiO<sub>2</sub>-Ag nanowires and their application in photocatalytic water splitting. *J. Mater. Chem. A* **2013**, *2* (8), 2648-2656.
10. Watté, J.; Lommens, P.; Pollefeyt, G.; Meire, M.; De Buysser, K.; Van Driessche, I., Highly Crystalline Nanoparticle Suspensions for Low-Temperature Processing of TiO<sub>2</sub> Thin Films. *ACS Appl. Mater. Interfaces* **2016**, *8* (20), 13027-13036.
11. Zhang, X.; Wang, H.; Xu, B.-Q., Remarkable Nanosize Effect of Zirconia in Au/ZrO<sub>2</sub> Catalyst for CO Oxidation. *The Journal of Physical Chemistry B* **2005**, *109* (19), 9678-9683.
12. Wang, H.; Chen, H.; Ni, B.; Wang, K.; He, T.; Wu, Y.; Wang, X., Mesoporous ZrO<sub>2</sub> Nanoframes for Biomass Upgrading. *ACS Appl. Mater. Interfaces* **2017**, *9* (32), 26897-26906.
13. De Roo, J.; Van Driessche, I.; Martins, J. C.; Hens, Z., Colloidal metal oxide nanocrystal catalysis by sustained chemically driven ligand displacement. *Nat Mater* **2016**, *15* (5), 517-521.
14. Lauria, A.; Villa, I.; Fasoli, M.; Niederberger, M.; Vedda, A., Multifunctional Role of Rare Earth Doping in Optical Materials: Nonaqueous Sol-Gel Synthesis of Stabilized Cubic HfO<sub>2</sub> Luminescent Nanoparticles. *ACS Nano* **2013**, *7* (8), 7041-7052.
15. Villa, I.; Vedda, A.; Fasoli, M.; Lorenzi, R.; Kränzlin, N.; Rechberger, F.; Ilari, G.; Primc, D.; Hattendorf, B.; Heiligtag, F. J.; Niederberger, M.; Lauria, A., Size-Dependent Luminescence in HfO<sub>2</sub> Nanocrystals: Toward White Emission from Intrinsic Surface Defects. *Chem. Mat.* **2016**, *28* (10), 3245-3253.
16. Joo, J.; Yu, T.; Kim, Y. W.; Park, H. M.; Wu, F. X.; Zhang, J. Z.; Hyeon, T., Multigranular scale synthesis and characterization of monodisperse tetragonal zirconia nanocrystals. *J. Am. Chem. Soc.* **2003**, *125* (21), 6553-6557.
17. Gordon, T. R.; Cargnello, M.; Paik, T.; Mangolini, F.; Weber, R. T.; Fornasiero, P.; Murray, C. B., Nonaqueous Synthesis of TiO<sub>2</sub> Nanocrystals Using TiF<sub>4</sub> to Engineer Morphology, Oxygen Vacancy Concentration, and Photocatalytic Activity. *J. Am. Chem. Soc.* **2012**, *134* (15), 6751-6761.
18. Cayado, P.; De Keukeleere, K.; Garzón, A.; Perez-Mirabet, L.; Meledin, A.; De Roo, J.; Vallés, F.; Mundet, B.; Rijckaert, H.; Pollefeyt, G.; Coll, M.; Ricart, S.; Palau, A.; Gázquez, J.; Ros, J.; Van Tendeloo, G.; Van Driessche, I.; Puig, T.; Obradors, X., Epitaxial YBa<sub>2</sub>Cu<sub>3</sub>O<sub>7</sub>-

x nanocomposite thin films from colloidal solutions. *Superconductor Science and Technology* **2015**, *28* (12), 124007.

19. Rijckaert, H.; Pollefeyt, G.; Sieger, M.; Hanisch, J.; Bennewitz, J.; De Keukeleere, K.; De Roo, J.; Huhne, R.; Backer, M.; Paturi, P.; Huhtinen, H.; Hemgesberg, M.; Van Driessche, I., Optimizing Nanocomposites through Nanocrystal Surface Chemistry: Superconducting YBa<sub>2</sub>Cu<sub>3</sub>O<sub>7</sub> Thin Films via Low-Fluorine Metal Organic Deposition and Preformed Metal Oxide Nanocrystals. *Chem. Mat.* **2017**, *29* (14), 6104-6113.

20. Maggiorrella, L.; Barouch, G.; Devaux, C.; Pottier, A.; Deutsch, E.; Bourhis, J.; Borghi, E.; Levy, L., Nanoscale radiotherapy with hafnium oxide nanoparticles. *Future Oncology* **2012**, *8* (9), 1167-1181.

21. Liu, C.; Hajagos, T. J.; Kishpaugh, D.; Jin, Y.; Hu, W.; Chen, Q.; Pei, Q., Facile Single-Precursor Synthesis and Surface Modification of Hafnium Oxide Nanoparticles for Nanocomposite  $\gamma$ -Ray Scintillators. *Adv. Funct. Mater.* **2015**, *25* (29), 4607-4616.

22. Cheema, T. A.; Garnweitner, G., Phase-controlled synthesis of ZrO<sub>2</sub> nanoparticles for highly transparent dielectric thin films. *Crystengcomm* **2014**, *16* (16), 3366-3375.

23. Liu, C.; Hajagos, T. J.; Chen, D.; Chen, Y.; Kishpaugh, D.; Pei, Q., Efficient One-Pot Synthesis of Colloidal Zirconium Oxide Nanoparticles for High-Refractive-Index Nanocomposites. *ACS Appl. Mater. Interfaces* **2016**, *8* (7), 4795-4802.

24. Molina, J.; Munoz, A. L.; Calleja, W.; Rosales, P.; Torres, A., High-quality spin-on glass-based oxide as a matrix for embedding HfO<sub>2</sub> nanoparticles for metal-oxide-semiconductor capacitors. *Journal of Materials Science* **2012**, *47* (5), 2248-2255.

25. Garnweitner, G.; Goldenberg, L. M.; Sakhno, O. V.; Antonietti, M.; Niederberger, M.; Stumpe, J., Large-scale synthesis of organophilic zirconia nanoparticles and their application in organic-inorganic nanocomposites for efficient volume holography. *Small* **2007**, *3* (9), 1626-1632.

26. Lee, S.; Shin, H.-J.; Yoon, S.-M.; Yi, D. K.; Choi, J.-Y.; Paik, U., Refractive index engineering of transparent ZrO<sub>2</sub>-polydimethylsiloxane nanocomposites. *J. Mater. Chem.* **2008**, *18* (15), 1751-1755.

27. Tao, P.; Li, Y.; Rungta, A.; Viswanath, A.; Gao, J.; Benicewicz, B. C.; Siegel, R. W.; Schadler, L. S., TiO<sub>2</sub> nanocomposites with high refractive index and transparency. *J. Mater. Chem.* **2011**, *21* (46), 18623-18629.

28. Wang, Y.; Fedin, I.; Zhang, H.; Talapin, D. V., Direct optical lithography of functional inorganic nanomaterials. *Science* **2017**, *357* (6349), 385-388.

29. De Roo, J.; De Keukeleere, K.; Hens, Z.; Van Driessche, I., From ligands to binding motifs and beyond; the enhanced versatility of nanocrystal surfaces. *Dalton Trans* **2016**, *45* (34), 13277-83.

30. Cozzoli, P. D.; Kornowski, A.; Weller, H., Low-temperature synthesis of soluble and processable organic-capped anatase TiO<sub>2</sub> nanorods. *J. Am. Chem. Soc.* **2003**, *125* (47), 14539-14548.

31. Buha, J.; Arcon, D.; Niederberger, M.; Djerdj, I., Solvothermal and surfactant-free synthesis of crystalline Nb<sub>2</sub>O<sub>5</sub>, Ta<sub>2</sub>O<sub>5</sub>, HfO<sub>2</sub>, and Co-doped HfO<sub>2</sub> nanoparticles. *Phys. Chem. Chem. Phys.* **2010**, *12* (47), 15537-15543.

32. Niederberger, M.; Bartl, M. H.; Stucky, G. D., Benzyl alcohol and titanium tetrachloride - A versatile reaction system for the nonaqueous and low-temperature preparation of crystalline and luminescent titania nanoparticles. *Chem. Mat.* **2002**, *14* (10), 4364-4370.

33. Pinna, N.; Garnweitner, G.; Antonietti, M.; Niederberger, M., Non-aqueous synthesis of high-purity metal oxide nanopowders using an ether elimination process. *Adv. Mater.* **2004**, *16* (23-24), 2196.

34. Zhou, S. X.; Garnweitner, G.; Niederberger, M.; Antonietti, M., Dispersion behavior of zirconia nanocrystals and their surface functionalization with vinyl group-containing ligands. *Langmuir* **2007**, *23* (18), 9178-9187.
35. De Roo, J.; De Keukeleere, K.; Feys, J.; Lommens, P.; Hens, Z.; Van Driessche, I., Fast, microwave-assisted synthesis of monodisperse HfO<sub>2</sub> nanoparticles. *J. Nanopart. Res.* **2013**, *15* (7), 1778.
36. Niederberger, M.; Garnweitner, G.; Krumeich, F.; Nesper, R.; Colfen, H.; Antonietti, M., Tailoring the surface and solubility properties of nanocrystalline titania by a nonaqueous in situ functionalization process. *Chem. Mat.* **2004**, *16* (7), 1202-1208.
37. Grote, C.; Cheema, T. A.; Garnweitner, G., Comparative Study of Ligand Binding during the Postsynthetic Stabilization of Metal Oxide Nanoparticles. *Langmuir* **2012**, *28* (40), 14395-14404.
38. De Roo, J.; Van den Broeck, F.; De Keukeleere, K.; Martins, J. C.; Van Driessche, I.; Hens, Z., Unravelling the Surface Chemistry of Metal Oxide Nanocrystals, the Role of Acids and Bases. *J. Am. Chem. Soc.* **2014**, *136* (27), 9650-9657.
39. De Keukeleere, K.; De Roo, J.; Lommens, P.; Martins, J. C.; Van der Voort, P.; Van Driessche, I., Fast and Tunable Synthesis of ZrO<sub>2</sub> Nanocrystals: Mechanistic Insights into Precursor Dependence. *Inorg. Chem.* **2015**, *54* (7), 3469-3476.
40. Trentler, T. J.; Denler, T. E.; Bertone, J. F.; Agrawal, A.; Colvin, V. L., Synthesis of TiO<sub>2</sub> nanocrystals by nonhydrolytic solution-based reactions. *J. Am. Chem. Soc.* **1999**, *121* (7), 1613-1614.
41. Depner, S. W.; Cultrara, N. D.; Farley, K. E.; Qin, Y.; Banerjee, S., Ferroelastic Domain Organization and Precursor Control of Size in Solution-Grown Hafnium Dioxide Nanorods. *ACS Nano* **2014**, *8* (5), 4678-4688.
42. Depner, S. W.; Kort, K. R.; Banerjee, S., Precursor control of crystal structure and stoichiometry in twin metal oxide nanocrystals. *Crystengcomm* **2009**, *11* (5), 841-846.
43. Tirosh, E.; Markovich, G., Control of defects and magnetic properties in colloidal HfO<sub>2</sub> nanorods. *Adv. Mater.* **2007**, *19* (18), 2608.
44. Tang, J.; Fabbri, J.; Robinson, R. D.; Zhu, Y. M.; Herman, I. P.; Steigerwald, M. L.; Brus, L. E., Solid-solution nanoparticles: Use of a nonhydrolytic sol-gel synthesis to prepare HfO<sub>2</sub> and Hf<sub>x</sub>Zr<sub>1-x</sub>O<sub>2</sub> nanocrystals. *Chem. Mat.* **2004**, *16* (7), 1336-1342.
45. Shaw, S.; Yuan, B.; Tian, X.; Miller, K. J.; Cote, B. M.; Colaux, J. L.; Migliori, A.; Panthani, M. G.; Cademartiri, L., Building Materials from Colloidal Nanocrystal Arrays: Preventing Crack Formation during Ligand Removal by Controlling Structure and Solvation. *Adv Mater* **2016**, *28* (40), 8892-8899.
46. Comparelli, R.; Fanizza, E.; Curri, M. L.; Cozzoli, P. D.; Mascolo, G.; Passino, R.; Agostiano, A., Photocatalytic degradation of azo dyes by organic-capped anatase TiO<sub>2</sub> nanocrystals immobilized onto substrates. *Applied Catalysis B: Environmental* **2005**, *55* (2), 81-91.
47. De Roo, J.; Coucke, S.; Rijckaert, H.; De Keukeleere, K.; Sinnaeve, D.; Hens, Z.; Martins, J. C.; Van Driessche, I., Amino Acid-Based Stabilization of Oxide Nanocrystals in Polar Media: From Insight in Ligand Exchange to Solution <sup>1</sup>H NMR Probing of Short-Chained Adsorbates. *Langmuir* **2016**, *32* (8), 1962-1970.
48. De Roo, J.; Justo, Y.; De Keukeleere, K.; Van den Broeck, F.; Martins, J. C.; Van Driessche, I.; Hens, Z., Carboxylic-Acid-Passivated Metal Oxide Nanocrystals: Ligand Exchange Characteristics of a New Binding Motif. *Angew. Chem.-Int. Edit.* **2015**, *54* (22), 6488-6491.
49. Shaw, S.; Colaux, J. L.; Hay, J. L.; Peiris, F. C.; Cademartiri, L., Building Materials from Colloidal Nanocrystal Arrays: Evolution of Structure, Composition, and Mechanical

Properties upon the Removal of Ligands by O<sub>2</sub> Plasma. *Adv Mater* **2016**, *28* (40), 8900-8905.

50. Shaw, S.; Silva, T. F.; Bobbitt, J. M.; Naab, F.; Rodrigues, C. L.; Yuan, B.; Chang, J. J.; Tian, X.; Smith, E. A.; Cademartiri, L., Building Materials from Colloidal Nanocrystal Assemblies: Molecular Control of Solid/Solid Interfaces in Nanostructured Tetragonal ZrO<sub>2</sub>. *Chem. Mat.* **2017**, *29* (18), 7888-7900.

51. Chen, P. E.; Anderson, N. C.; Norman, Z. M.; Owen, J. S., Tight Binding of Carboxylate, Phosphonate, and Carbamate Anions to Stoichiometric CdSe Nanocrystals. *J. Am. Chem. Soc.* **2017**, *139* (8), 3227-3236.

52. Kopping, J. T.; Patten, T. E., Identification of Acidic Phosphorus-Containing Ligands Involved in the Surface Chemistry of CdSe Nanoparticles Prepared in Tri-N-octylphosphine Oxide Solvents. *J. Am. Chem. Soc.* **2008**, *130* (17), 5689-5698.

53. Owen, J. S.; Park, J.; Trudeau, P. E.; Alivisatos, A. P., Reaction chemistry and ligand exchange at cadmium-selenide nanocrystal surfaces. *J. Am. Chem. Soc.* **2008**, *130* (37), 12279-12280.

54. Wang, F.; Tang, R.; Kao, J. L. F.; Dingman, S. D.; Buhro, W. E., Spectroscopic Identification of Tri-n-octylphosphine Oxide (TOPO) Impurities and Elucidation of Their Roles in Cadmium Selenide Quantum-Wire Growth. *J. Am. Chem. Soc.* **2009**, *131* (13), 4983-4994.

55. Wang, F. D.; Tang, R.; Buhro, W. E., The Trouble with TOPO; Identification of Adventitious Impurities Beneficial to the Growth of Cadmium Selenide Quantum Dots, Rods, and Wires. *Nano Lett.* **2008**, *8* (10), 3521-3524.

56. Anderson, N. C.; Hendricks, M. P.; Choi, J. J.; Owen, J. S., Ligand Exchange and the Stoichiometry of Metal Chalcogenide Nanocrystals: Spectroscopic Observation of Facile Metal-Carboxylate Displacement and Binding. *J. Am. Chem. Soc.* **2013**, *135* (49), 18536-18548.

57. Morris-Cohen, A. J.; Malicki, M.; Peterson, M. D.; Slavin, J. W. J.; Weiss, E. A., Chemical, Structural, and Quantitative Analysis of the Ligand Shells of Colloidal Quantum Dots. *Chem. Mat.* **2013**, *25* (8), 1155-1165.

58. Gomes, R.; Hassinen, A.; Szczygiel, A.; Zhao, Q. A.; Vantomme, A.; Martins, J. C.; Hens, Z., Binding of Phosphonic Acids to CdSe Quantum Dots: A Solution NMR Study. *J. Phys. Chem. Lett.* **2011**, *2* (3), 145-152.

59. Jun, Y.-w.; Casula, M. F.; Sim, J.-H.; Kim, S. Y.; Cheon, J.; Alivisatos, A. P., Surfactant-Assisted Elimination of a High Energy Facet as a Means of Controlling the Shapes of TiO<sub>2</sub> Nanocrystals. *J. Am. Chem. Soc.* **2003**, *125* (51), 15981-15985.

60. Pawsey, S.; McCormick, M.; De Paul, S.; Graf, R.; Lee, Y. S.; Reven, L.; Spiess, H. W., <sup>1</sup>H Fast MAS NMR Studies of Hydrogen-Bonding Interactions in Self-Assembled Monolayers. *J. Am. Chem. Soc.* **2003**, *125* (14), 4174-4184.

61. Pawsey, S.; Yach, K.; Reven, L., Self-Assembly of Carboxyalkylphosphonic Acids on Metal Oxide Powders. *Langmuir* **2002**, *18* (13), 5205-5212.

62. De Roo, J.; Baquero, E. A.; Coppel, Y.; De Keukeleere, K.; Van Driessche, I.; Nayral, C.; Hens, Z.; Delpech, F., Insights into the Ligand Shell, Coordination Mode, and Reactivity of Carboxylic Acid Capped Metal Oxide Nanocrystals. *ChemPlusChem* **2016**, *81* (11), 1216-1223.

63. Wolcott, A.; Fitzmorris, R. C.; Muzaffery, O.; Zhang, J. Z., CdSe Quantum Rod Formation Aided By In Situ TOPO Oxidation. *Chem. Mat.* **2010**, *22* (9), 2814-2821.

64. Vioux, A., Nonhydrolytic sol-gel routes to oxides. *Chem. Mat.* **1997**, *9* (11), 2292-2299.

65. Niederberger, M.; Garnweitner, G., Organic reaction pathways in the nonaqueous synthesis of metal oxide nanoparticles. *Chem.-Eur. J.* **2006**, *12* (28), 7282-7302.
66. Cook, A. G.; Mason, G. W., Structural effects on the acid-base properties of some closely related phosphinic acids and phosphine oxides. *The Journal of Organic Chemistry* **1972**, *37* (21), 3342-3345.
67. Kim, K.; Yoo, D.; Choi, H.; Tamang, S.; Ko, J. H.; Kim, S.; Kim, Y. H.; Jeong, S., Halide-Amine Co-Passivated Indium Phosphide Colloidal Quantum Dots in Tetrahedral Shape. *Angew Chem Int Ed* **2016**, *55* (11), 3714-8.
68. Gabka, G.; Bujak, P.; Gryszel, M.; Ostrowski, A.; Malinowska, K.; Zukowska, G.; Agnese, F.; Pron, A.; Reiss, P., Facile synthesis and surface chemistry of high quality wurtzite and kesterite Cu<sub>2</sub>ZnSnS<sub>4</sub> nanocrystals using tin(II) 2-ethylhexanoate as a new tin source. *Chem. Commun.* **2015**.
69. Mourdikoudis, S.; Liz-Marzan, L. M., Oleylamine in Nanoparticle Synthesis. *Chem. Mat.* **2013**, *25* (9), 1465-1476.
70. Liu, Y.; Cadavid, D.; Ibanez, M.; De Roo, J.; Ortega, S.; Dobrozhan, O.; V. Kovalenko, M.; Cabot, A., Colloidal AgSbSe<sub>2</sub> nanocrystals: surface analysis, electronic doping and processing into thermoelectric nanomaterials. *Journal of Materials Chemistry C* **2016**, *4* (21), 4756-4762.
71. Berestok, T.; Guardia, P.; Blanco, J.; Nafria, R.; Torruella, P.; Lopez-Conesa, L.; Estrade, S.; Ibanez, M.; de Roo, J.; Luo, Z.; Cadavid, D.; Martins, J. C.; Kovalenko, M. V.; Peiro, F.; Cabot, A., Tuning Branching in Ceria Nanocrystals. *Chem. Mat.* **2017**, *29* (10), 4418-4424.
72. Zheng, A.; Huang, S.-J.; Liu, S.-B.; Deng, F., Acid properties of solid acid catalysts characterized by solid-state <sup>31</sup>P NMR of adsorbed phosphorous probe molecules. *Phys. Chem. Chem. Phys.* **2011**, *13* (33), 14889-14901.
73. Zhao, Q.; Chen, W.-H.; Huang, S.-J.; Wu, Y.-C.; Lee, H.-K.; Liu, S.-B., Discernment and Quantification of Internal and External Acid Sites on Zeolites. *The Journal of Physical Chemistry B* **2002**, *106* (17), 4462-4469.
74. Chen, W.-H.; Ko, H.-H.; Sakthivel, A.; Huang, S.-J.; Liu, S.-H.; Lo, A.-Y.; Tsai, T.-C.; Liu, S.-B., A solid-state NMR, FT-IR and TPD study on acid properties of sulfated and metal-promoted zirconia: Influence of promoter and sulfation treatment. *Catal. Today* **2006**, *116* (2), 111-120.
75. Corma, A., Inorganic Solid Acids and Their Use in Acid-Catalyzed Hydrocarbon Reactions. *Chem. Rev.* **1995**, *95* (3), 559-614.
76. Melero, J. A.; Iglesias, J.; Morales, G., Heterogeneous acid catalysts for biodiesel production: current status and future challenges. *Green Chem.* **2009**, *11* (9), 1285-1308.
77. Niu, Z.; Li, Y., Removal and Utilization of Capping Agents in Nanocatalysis. *Chem. Mat.* **2014**, *26* (1), 72-83.
78. Wu, Z.; Jiang, D. E.; Mann, A. K.; Mullins, D. R.; Qiao, Z. A.; Allard, L. F.; Zeng, C.; Jin, R.; Overbury, S. H., Thiolate ligands as a double-edged sword for CO oxidation on CeO<sub>2</sub> supported Au<sub>25</sub>(SCH<sub>2</sub>CH<sub>2</sub>Ph)<sub>18</sub> nanoclusters. *J. Am. Chem. Soc.* **2014**, *136* (16), 6111-22.
79. Pujari, S. P.; Scheres, L.; Marcelis, A. T. M.; Zuilhof, H., Covalent Surface Modification of Oxide Surfaces. *Angewandte Chemie International Edition* **2014**, *53* (25), 6322-6356.
80. Paniagua, S. A.; Giordano, A. J.; Smith, O. L.; Barlow, S.; Li, H.; Armstrong, N. R.; Pemberton, J. E.; Bredas, J. L.; Ginger, D.; Marder, S. R., Phosphonic Acids for Interfacial Engineering of Transparent Conductive Oxides. *Chem Rev* **2016**, *116* (12), 7117-58.
81. Manzer, L. E.; Deaton, J.; Sharp, P.; Schrock, R. R., 31. Tetrahydrofuran Complexes of Selected Early Transition Metals. In *Inorganic Syntheses*, John Wiley & Sons, Inc.: 2007; pp 135-140.

82. Hens, Z.; Martins, J. C., A Solution NMR Toolbox for Characterizing the Surface Chemistry of Colloidal Nanocrystals. *Chem. Mat.* **2013**, *25* (8), 1211-1221.
83. Akoka, S.; Barantin, L.; Trierweiler, M., Concentration Measurement by Proton NMR Using the ERETIC Method. *Anal. Chem.* **1999**, *71* (13), 2554-2557.
84. Connell, M. A.; Bowyer, P. J.; Bone, P. A.; Davis, A. L.; Swanson, A. G.; Nilsson, M.; Morris, G. A., Improving the accuracy of pulsed field gradient NMR diffusion experiments: Correction for gradient non-uniformity. *J. Magn. Reson.* **2009**, *198* (1), 121-131.

# TOC graphic

